Strain dependence of peak widths of reciprocal- and real-space distribution functions of metallic glasses from *in situ* x-ray scattering and molecular dynamics simulations

R. T. Ott,[1] M. I. Mendelev,[1] M. F. Besser,[1] M. J. Kramer,[1,2] J. Almer,[3] and D. J. Sordelet[1]
[1]*Materials Science and Engineering, Ames Laboratory, U.S. DOE, Ames, Iowa 50011, USA*
[2]*Department of Materials Science and Engineering, Iowa State University, Ames, Iowa 50011, USA*
[3]*Argonne National Laboratory, Advanced Photon Source, Argonne, Illinois 60439, USA*
(Received 4 March 2009; revised manuscript received 15 June 2009; published 4 August 2009)

We have examined the relationship between the variance in the atomic-level hydrostatic pressure, $\langle \Delta p^2 \rangle^{1/2}$, and the widths of the first peaks in the reciprocal- and real-space distribution functions for elastically deformed metallic glasses. *In situ* synchrotron x-ray scattering studies performed on a binary $Cu_{64.5}Zr_{35.5}$ glass subject to uniaxial loading reveal that the width of the first peak in the reduced-pair distribution function is dependent on the different elastic responses of the partial-pair correlations. Molecular dynamics (MD) simulations of the same binary glass, as well as a single-component glass, subject to hydrostatic deformation show that the widths of the first peaks in the partial-pair distribution functions are affected by length-scale-dependent changes in the relative atomic separation in the first nearest-neighbor shell. Moreover, the MD simulations show that the strain dependencies of the partial-pair peak widths do not necessarily match the strain-dependence of $\langle \Delta p^2 \rangle^{1/2}$. The results suggest that the widths of the peaks in the reciprocal- and real-space functions are not solely dependent on $\langle \Delta p^2 \rangle^{1/2}$ but rather are also affected by the atomic rearrangements associated with elastic deformation.

DOI: 10.1103/PhysRevB.80.064101 PACS number(s): 61.43.Dq, 61.43.Bn, 61.05.cf, 83.50.−v

I. INTRODUCTION

The structural aspects involved in the elastic deformation of metallic glasses differ from those of crystalline materials in which the atoms are confined by the symmetry of the lattice. Despite the disordered nature of the atomic structure of metallic glasses, x-ray and neutron scattering can be utilized to examine the atomic-scale elastic deformation behavior of metallic glasses.[1–5] In particular, changes in atomic separations associated with elastic deformation of a metallic glass can be determined from the shifts in the peaks of the reciprocal- and real-space distribution functions. Moreover, by utilizing a two-dimensional (2D) area detector, the atomic separations in two principal directions (parallel and normal to the loading axis) can be measured simultaneously. The widths of the first peaks in the reciprocal- and real-space distribution functions have also been reported to be dependent on the applied stress.[2,3] For instance, Hufnagel *et al.*[2] examined the stress dependence of the radial distribution function (RDF) peak width for a Zr-Cu-Ni-Al-Ti metallic glass loaded in uniaxial compression. Using a two-Gaussian-peak model to fit the first shell, they found that the peak widths of the RDF corresponding to atomic correlations along the longitudinal direction (parallel to loading axis) decreased with increasing compressive stress, while the peak widths in the transverse direction (normal to loading axis) increased with increasing compressive stress. Interestingly, the magnitude of the increase in the peak widths in the transverse direction were less than the decrease in the longitudinal direction by a factor approximately equal to Poisson's ratio. Moreover, Das *et al.*[3] examined the strain dependence of the width of the first peak in the total structure factor, $S(Q)$, for a similar Zr-based metallic glass and a ternary Zr-Cu-Al glass loaded in uniaxial compression. From their *in situ* measurements, they found that the width of the first peak in $S(Q)$ for the longitudinal direction decreased with increasing compressive stress and increased, to a lesser extent, for the transverse direction. In both studies, the overall decrease in peak widths for the reciprocal- and real-space functions was attributed to a decrease in the variance of the atomic-level hydrostatic pressure distribution.

The importance of atomic-level stresses in describing the structure of amorphous solids has been previously shown by Egami *et al.*[6] The local hydrostatic pressure, p, describes the local-density fluctuations and is simply defined as

$$p = -\frac{1}{3}(\sigma_1 + \sigma_2 + \sigma_3), \tag{1}$$

where σ_1, σ_2, and σ_3 are the three principal stresses.[7] While the average hydrostatic pressure, $\langle p \rangle$, of the system tends to zero, the variance of the local hydrostatic pressure, $\langle \Delta p^2 \rangle^{1/2}$, has been found to approach 6% of the bulk modulus.[8] Srolovitz and co-workers[8] examined the relationship between the pair-distribution function, $g(r)$, and the hydrostatic pressure variance for a single-component model amorphous structure containing 2067 atoms[9] with a modified Johnson potential[10] for iron. To study the effects of the local-density fluctuations on $g(r)$, they divided the p distribution into three sections; one section each for the 25% of the atoms subject to largest compressive and tensile pressures, respectively, and the third section corresponding to the remaining atoms with the smallest hydrostatic pressures. To examine the effects of annealing, they excluded the atoms in the two edge sections in the p distribution and calculated $g(r)$ by successively centering the origin on only the atoms that corresponded to the central section of the p distribution. From their analysis, they determined that the width of the first peak in the $g(r)$ decreased as the variance in p decreased. It should be noted that the models examined in the work above were not strained, therefore, the affects of applied strain on $\langle \Delta p^2 \rangle^{1/2}$ and the peak widths were not examined.

The physical nature of the distribution-function-peak width changes during deformation remains unclear. In the current study, we examine the relationship between the variance in the local hydrostatic pressure and the widths of the first peaks in the reciprocal- and real-space distribution functions for elastically deformed metallic glasses. Using *in situ* synchrotron x-ray scattering we studied a binary $Cu_{64.5}Zr_{35.5}$ glass subject to uniaxial compression and tension. The experimental observations were compared to molecular dynamics (MD) simulations of the same binary glass subject to uniaxial and hydrostatic deformation, as well as a single-component glass deformed hydrostatically. From both the x-ray and MD results we find that the widths of the first peaks in the total-distribution functions are strongly dependent on the different elastic responses of the partial-pair correlations. Furthermore, we find that the widths of the first peaks in the partial-pair distribution functions can exhibit strain dependencies different than that of the total-pair distribution function. The results suggest that the widths of the peaks in the reciprocal- and real-space functions are not solely dependent on $\langle \Delta p^2 \rangle^{1/2}$. The nature of the atomic displacements that result in the different strain dependencies of the peak widths is discussed.

II. EXPERIMENTAL AND NUMERICAL TECHNIQUES

A. Sample preparation

Alloy ingots of nominal composition $Cu_{64.5}Zr_{35.5}$ were prepared by arc melting pure elements in an Ar environment. The ingots, which were melted and flipped several times to promote homogeneity, were cast into a 10-mm-diameter Cu mold.[11] Approximately 12 g of the as-cast rod was cut and melted in a graphite tube to prepare ribbons by melt spinning using a single-roller Cu wheel with a linear surface velocity of 10 m/s. The ribbons for the tensile experiments were approximately 4 mm wide and 100 μm in thickness. For the compression experiments, rods were prepared by injection casting $\sim$1 g of the cast $Cu_{64.5}Zr_{35.5}$ 10 mm rod into a Cu mold 1.2 mm in diameter and 40 mm in length. The rods were subsequently ground to $\sim$1 mm in diameter to assure a cylindrical cross section and cut to a length:diameter ratio of 2:1. Lastly, the ends were polished in a jig to ensure parallelism.

B. *In situ* x-ray scattering

The *in situ* x-ray experiments were performed at the 1-ID beamline of the Advanced Photon Source at Argonne National Laboratory. Monochromatic 85.980 keV (λ =0.01442 nm) x-rays were used for the experiments performed in transmission mode. The samples were loaded in a MTS model 858 load frame mounted on a translation stage to allow for movement of the sample in the plane normal to the beam direction. A GE amorphous Si detector with a pixel size of 200$\times$200 μm was placed 362 mm downstream from the samples to record the scattered intensity out to a Q-range of $\sim$20 Å^{-1} ($Q=4\pi \sin\theta/\lambda$). The 2D images were azimuthally binned into slices of 6° and the scattering patterns (intensity versus scattering vector) corresponding to the longitudinal (loading axis) and the transverse directions were extracted by integrating the bins that fall between $\pm 9°$ about the principal axes using the software package FIT2D.[12]

For the tensile experiments, the samples were loaded in increments of 50 MPa and held at each load to acquire ten images with 1 s exposure times. The ten images for each loading step were averaged and then integrated as described above. To measure the macroscopic strain along the loading axis, a strain gage was attached to the tensile samples. For the compression experiments, the experiments were done in real time at a constant strain rate of $\sim 2\times 10^{-4}$ s^{-1}. Exposures were obtained during loading at a frequency of 1 Hz. For the high-temperature compression experiments the samples were heated in an infrared furnace to 425 °C and deformed at a constant strain rate of 10^{-4} s^{-1}. Prior to loading the samples for both the compressive and tensile tests were annealed at 375 °C for 270 min to allow for structural relaxation.

For the integrated diffraction patterns, $I(Q)$, corresponding to the longitudinal and transverse directions, the scans were corrected for absorption, polarization, multiple scattering, and Compton scattering using the PDFGETX2 software[13–18] and the total structure factor, $S(Q)$, was calculated according to

$$S(Q) = 1 + \frac{\left[I(Q) - \sum_{i=1}^{n} a_i |f_i(Q)|^2 \right]}{\left| \sum_{i=1}^{n} a_i f_i(Q) \right|^2}, \quad (2)$$

where a_i is the atomic fraction of each element and f_i is the Q-dependent scattering factor for each element.

The real-space reduced-pair-distribution function, $G(r)$, was calculated by Fourier transforming the total structure factor as follows:

$$G(r) = 4\pi r[\rho(r) - \rho_o] = \frac{2}{\pi}\int_0^\infty [S(Q) - 1]\sin(Qr)dQ, \quad (3)$$

where $\rho(r)$ is the atomic density at a distance r away from an average atom located at the origin and ρ_o is the average atomic density. It should be noted that Eq. (3) assumes that the glass is isotropic, which is not the case for a glass subject to uniaxial loading. Dmowski and co-workers[19] found that the correction is not overly large for thermomechanically induced bond-length anisotropy, therefore, we did not use spherical harmonics to calculate the distribution functions for the longitudinal and transverse directions. Furthermore, the cylindrical geometry of the compression samples was not considered in the absorption- and multiple-scattering corrections, however, we did check the results against selected scans that were corrected for the cylindrical geometry and found that the differences between the measured peak widths using the flat plate geometry and the cylindrical geometry were all $<0.01\%$.

C. Molecular dynamics simulations

We performed MD simulations of two glass systems, amorphous Cu-Zr and Al, subject to deformation. The mod-

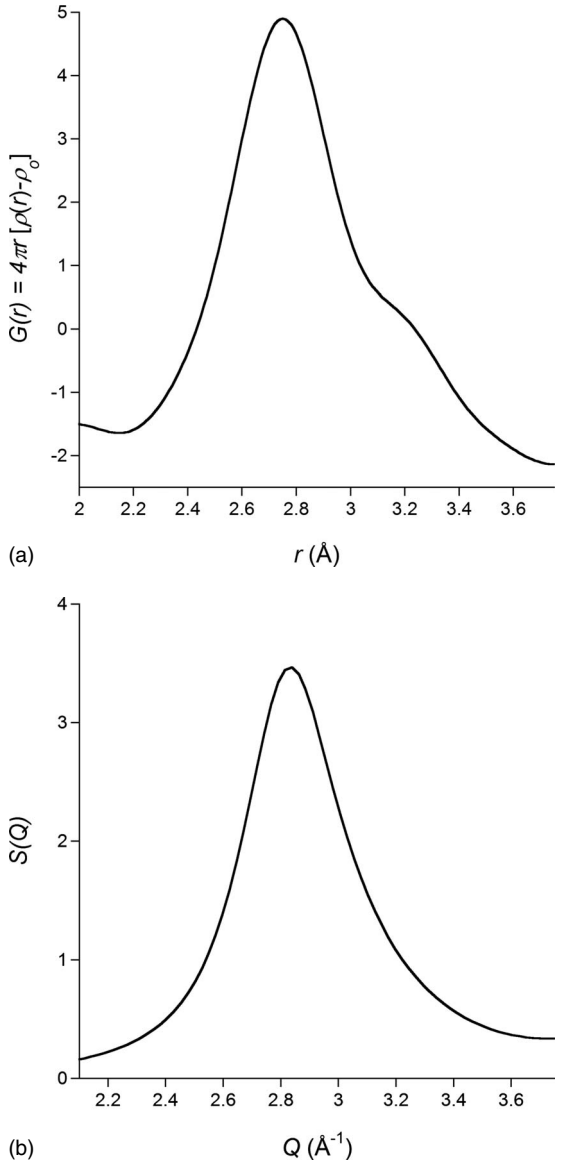

FIG. 1. First peak in the total (a) $G(r)$ and (b) $S(Q)$ for the longitudinal direction of a $Cu_{64.5}Zr_{35.5}$ alloy under small tensile load.

els of amorphous $Cu_{64.5}Zr_{35.5}$ and $Cu_{33.3}Zr_{66.7}$ alloys were created using the interatomic potential from Ref. 20. The details of the MD simulations can be found in Ref. 21. The details of the creation of the one-component model described by the Ercolessi-Adams Al potential[22] and some its properties are described in Ref. 23. For the $Cu_{64.5}Zr_{35.5}$ model we simulated uniaxial deformation for comparison with the experimental measurements. Unlike the experiments in which there are free surfaces normal to the loading axis, it is not reasonable to utilize free surfaces in the simulations since the surface effect would be very large for a relatively small model with dimensions of ~4 nm. Therefore, in our simulations the model had periodic boundary conditions in all directions. The model size in the z direction was changed according to the chosen value of the applied strain ε_{zz} while the model size in the x and y directions was chosen such that $\sigma_{xx}=\sigma_{yy}=0$. We performed 20 000 MD steps (~40.7 ps) to equilibrate the models. Since the applied strain is not isotropic, directional-pair-distribution functions were calculated. For the longitudinal direction only pairs with angle not larger than $\pm 9°$ from the z axis were included in the directional-pair-distribution function and for the transverse direction only pairs with angle not larger than $\pm 9°$ from the xy plane were included in the directional-pair-distribution function. Thus only 1.2% and 15.6% of pairs were used to obtain the longitudinal and transverse functions, respectively. Obviously, the statistics for the longitudinal functions are worse than that for the transverse functions. All pair-distribution functions were averaged during the next 200 000 MD steps after each applied strain.

To simulate hydrostatic deformation ($\varepsilon_{xx}=\varepsilon_{yy}=\varepsilon_{zz}$; $\varepsilon_{xy}=\varepsilon_{yz}=\varepsilon_{xz}=0$) in all three models, we changed the model size according to the chosen value of ε, performed 20 000 MD steps and then averaged the model partial-pair distribution functions during the next 200 000 MD steps. The pair-distribution functions were calculated using as step size 0.025 Å for both systems. The structure factor for the Al glass was calculated via inverse Fourier transformation of the pair-distribution function using a step size of 0.025 $Å^{-1}$.

The atomic pressure, p_i, in each model was calculated according to

$$p_i = \frac{kT_i}{V/N} + \frac{1}{3V/N}\sum_{j=i+1}^{N} F_{ij}r_{ij}, \tag{4}$$

where k is Boltzman's constant, T_i is the temperature of atom i, F_{ij} is the force acting on atom i from atom j, r_{ij} is the distance between atom i and j, and V/N is the average atomic volume. From this, the variance in the hydrostatic pressure was calculated from

$$\langle \Delta p^2 \rangle^{1/2} = \sqrt{\frac{1}{N}\sum_{i=1}^{N}(p_i - p)^2}, \tag{5}$$

for which p is the pressure in the model.

III. RESULTS AND DISCUSSION

A. Peak widths from *in situ* x-ray scattering

The first peaks of the total $G(r)$ and $S(Q)$ functions (longitudinal direction) measured by x-ray scattering for a $Cu_{64.5}Zr_{35.5}$ sample under a small tensile load are shown in Fig. 1. The shape of the peaks in both functions raises the important question of how peak widths are measured. While the first peak in the total $S(Q)$ appears to be reasonably symmetric, it is in fact a convolution of the three partial-pair structure factors for the binary glass. The convolution of the three partial pairs is more clearly seen in the first peak of the total $G(r)$, which corresponds to the real-space description of Cu-Cu, Cu-Zr, and Zr-Zr bond distances within the first nearest-neighbor atomic shell. The low-r side of the first peak centered at ~2.8 Å shows a higher intensity peak corresponding to primarily Cu-Cu and Cu-Zr correlations while the shoulder on the high-r side at ~3.2 Å can be attributed to Zr-Zr correlations. The assignment of the partial-pair correlations to the low- and high-r sides of the first peak is

based on the MD simulations of the alloy.[20] Due to the obvious asymmetry of the first peak in the total $G(r)$, a single-peak profile cannot be used to determine the width. One approach is to use a three-peak model to fit the individual partial-pair correlations but without any additional constraints accurately measuring small changes in the peak widths is difficult due to the large number of variable parameters associated with fitting three peaks. An alternative to fitting the data to specified peak profiles is to measure the r values at which $G(r)$ crosses some specified value (e.g., $G(r)=0$ Å^{-2}). The peak width is then simply defined as the difference of the two intercept points. On the one hand this method does not allow us to measure the peak widths of the individual partial pairs. On the other hand, it is rather sensitive to small changes in the peak width of the total $G(r)$. Selecting the appropriate intercept points to define the peak width should not be arbitrary, however, since the measurements are dependent on which partial-pair correlations are being sampled. For example, if the intercept points are chosen where $G(r)=4$ Å^{-2}, then the Zr-Zr correlations are not likely being included since $G_{\text{Zr-Zr}}(r)$ is lower in intensity than $G_{\text{Cu-Cu}}(r)$ an $G_{\text{Cu-Zr}}(r)$. For measuring the width of the first peak in the total $G(r)$ in the current study, we chose $G(r)=0$ Å^{-2} as the intercept value since all three partial-pair correlations and the total $G(r)$ oscillate around this value. Likewise, the width of the first peak in the total $S(Q)$ was defined as the difference between the two intercept points where $S(Q)=1$. The measured widths of the first peaks in the total $G(r)$ and $S(Q)$ as functions of applied stress for the $Cu_{64.5}Zr_{35.5}$ metallic glass are shown in Fig. 2. Note, the data in Fig. 2 are a combination of measurements in uniaxial tension for the melt-spun ribbons and uniaxial compression for the injection-cast rods. For $G(r)$, the peak width appears to exhibit a more or less linear stress dependence. For the longitudinal direction (parallel to loading axis) the peak width decreases for compressive loading and increases for tensile loading. In contrast, the $G(r)$ peak width in the transverse direction (normal to loading axis) increases for compressive loading and decreases for tensile loading. The slope of the stress dependence of the peak widths in the transverse direction is smaller than the stress dependence in the longitudinal direction by a factor close to the reported Poisson's ratio for the compositionally similar $Cu_{66}Zr_{34}$ metallic glass [0.36 vs $\nu=0.352$ (Ref. 24)].

The measured width of the first peak in the total $S(Q)$ also exhibits an approximately linear dependence on the applied stress. Similar to the total $G(r)$, the stress dependence of the peak widths corresponding to correlations along the longitudinal direction is larger than the stress dependence of the peak widths for correlations along the transverse direction. The peak widths of the total $S(Q)$, however, respond in an opposite manner than the peak widths for the total $G(r)$; the $S(Q)$ peak width in the longitudinal direction increases with compressive loading and decreases with tensile loading while the peak width in the transverse direction decreases for compressive loading and increases for tensile loading.

The opposite stress dependencies of the peak widths for $G(r)$ and $S(Q)$ highlight the problems associated with extracting peak widths from total-distribution functions. A key assumption for peak widths measured using the intercept method is that all atoms, on average, respond equivalently to an applied stress. This is highly unlikely, however, given the variance in the bond stiffnesses for the different atoms in the amorphous alloy. To check the validity of this assumption for the $Cu_{64.5}Zr_{35.5}$ metallic glass, we calculated the atomic-scale strain from the different intercept points. For the real-space data, the strain is simply defined as

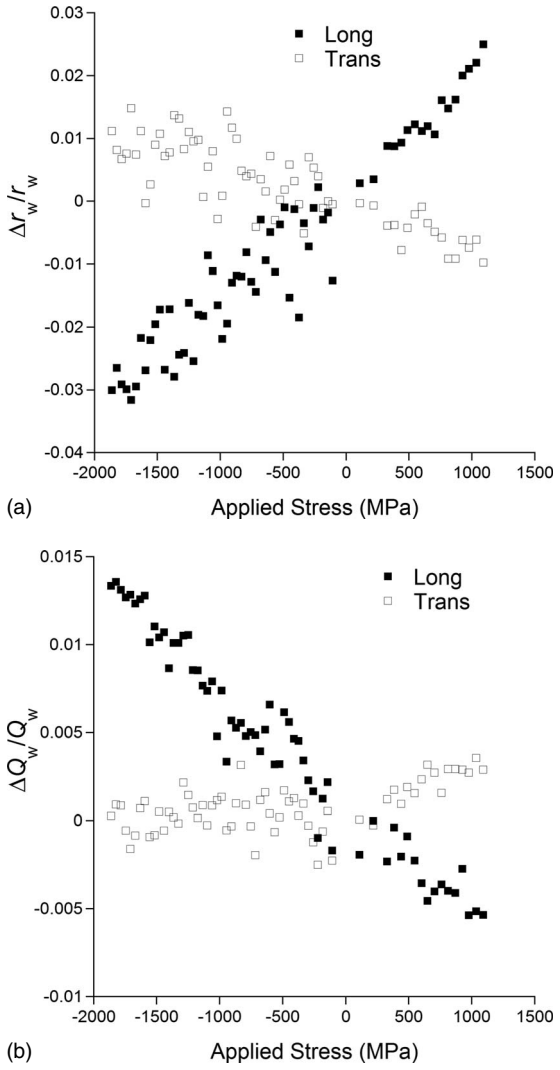

FIG. 2. Normalized widths of first peaks in total (a) $G(r)$ and (b) $S(Q)$ measured by *in situ* x-ray scattering as functions of applied uniaxial stress.

$$\varepsilon = \frac{r_i^s - r_i^o}{r_i^o}, \tag{6}$$

where r_i^s and r_i^o are the radial positions corresponding to $G(r)=0$ Å^{-2} for a strained and unstrained sample, respectively. For the reciprocal-space data the strain is defined as

$$\varepsilon = \frac{\frac{1}{Q_i^s} - \frac{1}{Q_i^o}}{\frac{1}{Q_i^o}}, \tag{7}$$

where Q_i^s and Q_i^o are the Q positions corresponding to $S(Q)=1$ for a strained and an unstrained sample, respectively. Since there are two intercept points for the first peaks in the distribution functions, we will refer to the intercepts at low-Q and low-r values as Q_1 and r_1, respectively, similarly the intercepts at high-Q and high-r values will be identified as Q_2 and r_2, respectively, from hereon in. It should be noted that Eqs. (6) and (7) assume that the atoms exhibit a uniform displacement, that is, proportional to the macroscopic strain. This however, is not very likely since relaxation events that are not purely elastic in nature can occur during straining as has been observed in previous computational studies.[25,26] Therefore, there is no inherent reason that the atomic-scale strain calculated from the displacement of the peaks in the distribution functions should be equal to the macroscopic strain. Figure 3 shows the atomic-scale strain in the longitudinal direction as a function of applied stress calculated from the $G(r)$ and $S(Q)$ intercepts along with the macroscopic strain measured via a strain gage attached to the sample, which was loaded in uniaxial tension. For the total $G(r)$, we find that the strain calculated from the low-r intercept (r_1) agrees well with the macroscopic strain measured by a strain gage, while the strain calculated from the high-r intercept (r_2) is higher than the macroscopic strain. Since the high-r side of the first peak corresponds to Zr-Zr correlations, the strain calculated from r_2 is primarily dependent on the change in the relative atomic separations of the Zr-Zr atomic pairs. From our previous MD simulations we have found that the Zr-Zr correlations are significantly more compliant than the Cu-Cu and Cu-Zr correlations,[21] which is why the strain calculated from r_2 is greater than the strain calculated from r_1. The different strain responses of the r_1 and r_2 intercepts directly influence the measured peak widths for the total $G(r)$. For the longitudinal direction, the higher strain calculated from r_2 means the relative change in the position of the r_2 intercept is larger than that of the r_1 intercept. Therefore, the distance between the two intercepts (peak width) should be less than in the unstrained state for compressive loading and greater than the unstrained state for tensile loading, which is consistent with what we observe experimentally.

For the reciprocal-space data in Fig. 3(b), the stress dependence of the strain calculated from Q_1 is larger than that of the strain calculated from Q_2. From the total and partial $S(Q)$s determined by MD simulations of the $Cu_{64.5}Zr_{35.5}$ alloy (not shown) we find that the low-Q side of the first peak in the total $S(Q)$ corresponds primarily to contributions from $S_{Zr\text{-}Zr}(Q)$ and the high-Q side of the first peak in the total $S(Q)$ corresponds primarily to $S_{Cu\text{-}Cu}(Q)$. Therefore, the strain response calculated from Q_1 should be larger than Q_2 since the Zr-Zr correlations are more compliant. As with the real-space data, the different stress dependencies of the strains calculated from Q_1 and Q_2 affects the measured peak width, however, the different strain responses of the intercept points would cause the peak widths in the longitudinal direction to decrease for compressive loading and increase for tensile loading, which is opposite of what we measured in Fig. 2. This behavior suggest that there are competing factors influencing the peak widths, which might be related to the fact that the magnitude of peak width changes for $S(Q)$ are smaller than those measured for $G(r)$.

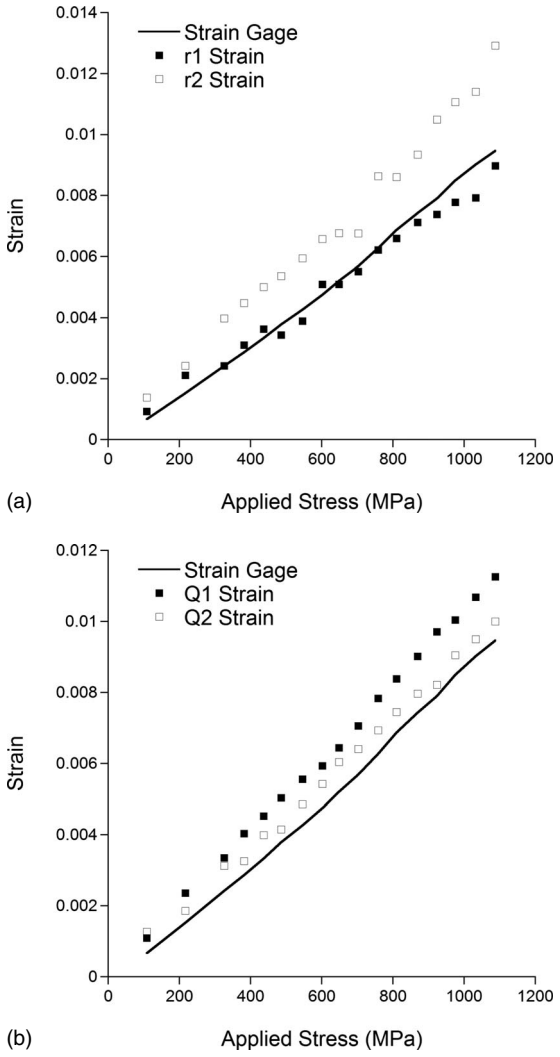

FIG. 3. Atomic strains in longitudinal direction calculated from the intercept points of the first peaks in the total (a) $G(r)$ and (b) $S(Q)$. The macroscopic strain along the loading axis, which was measured by a strain gage, is also shown. For the x-ray measurements, r_1 and Q_1 represent the strain calculated from the intercept points on the left side of the peaks and r_2 and Q_2 represent strains calculated from the intercept points on the right side of the peaks.

B. Molecular dynamics simulations of uniaxial deformation

The results in Fig. 2 show that the width of the first peak in the total $G(r)$ is indeed dependent on the applied stress; however, the different strains exhibited by the two intercept points (Fig. 3) reveal that the widths of the partial-pair correlations need to be considered since the width of the total $G(r)$ is affected by the displacements of the partial-pair func-

tions. Furthermore, the *in situ* x-ray measurements do not reveal anything about the stress(strain) dependence of $\langle \Delta p^2 \rangle^{1/2}$. Therefore, to examine the influence of elastic deformation on the variance in the local hydrostatic pressure and the peak widths of partial-pair distribution functions, we performed MD simulations of the $Cu_{64.5}Zr_{35.5}$ binary glasses subject to uniaxial deformation. Since the atomic density is known in the MD simulations, for each atomic configuration it is straightforward to calculate the partial-pair distribution functions, $g_{\alpha\beta}(r)$, which can be expressed as

$$g_{\alpha\beta}(r) = \frac{\rho_{\alpha\beta}(r)}{\rho_o} = \frac{G_{\alpha\beta}(r)}{4\pi r \rho_o} + 1, \tag{8}$$

where $\rho_{\alpha\beta}$ is the atomic density of β atoms around a central α atom and ρ_o is the average atomic density. This is related to the total-pair distribution function, $g(r)$, according to

$$g(r) = x_1^2 k_1^2 g_{11} + 2x_1 x_2 k_1 k_2 g_{12} + x_2^2 k_2^2 g_{22}, \tag{9}$$

where x_α is the atomic fraction of the αth component, k is the weighting factor of the αth component, which is defined as

$$k_\alpha = \frac{f_\alpha}{x_1 f_1 + x_2 f_2}, \tag{10}$$

for which f_α is the atomic scattering factor of the α component using the Faber-Ziman formalism. For comparison with the x-ray results, the peak width in the total $g(r)$ as a function of applied strain was determined by taking the difference between the two intercept points where $g(r)=1$. The intercept method was also utilized to measure the peak widths of the partial-pair distribution functions since different elastic responses should not be prevalent in the individual partial-pair functions. Furthermore, the peaks in the partial-pair distribution functions can exhibit significant asymmetry, which makes fitting to a single profile unreliable.

The first peak in the $g(r)$ for the unstrained $Cu_{64.5}Zr_{35.5}$ model along with its measured width as a function of applied uniaxial strain is shown in Fig. 4. Similar to the *in situ* x-ray experiments, the width of the first peak in the longitudinal direction decreases for compressive straining and increases for tensile straining. For the transverse direction, the peak widths exhibit opposite dependence on the applied uniaxial strain and the magnitude of the changes are less compared to the longitudinal direction, which is also consistent with the experiments. It should be noted however, that if we plot the peak widths as functions of the strain along the principal directions where $\varepsilon_{zz}=\varepsilon_{app}$, $\varepsilon_{xx}=\varepsilon_{yy}=-\upsilon\varepsilon_{zz}$, and $\varepsilon_{xy}=\varepsilon_{yz}=\varepsilon_{xz}=0$, then we get very similar strain dependencies for the peak widths, Fig. 4(c). To check if the changes in peak widths for the principal directions were dependent on the difference in the elastic responses of the partial-pair correlations, the strain from the shifts in the r_1 and r_2 intercepts were calculated for the longitudinal and transverse directions, Fig. 5. As was the case for the $Cu_{64.5}Zr_{35.5}$ ribbon tested in uniaxial tension, the strain calculated from the shifts in the r_2 intercept is larger than the strain calculated from the shifts in the r_1 intercept. As discussed above, the r_1 intercept corresponds primarily to Cu-Cu correlations and the r_2 intercept corresponds to the more compliant Zr-Zr correlations.

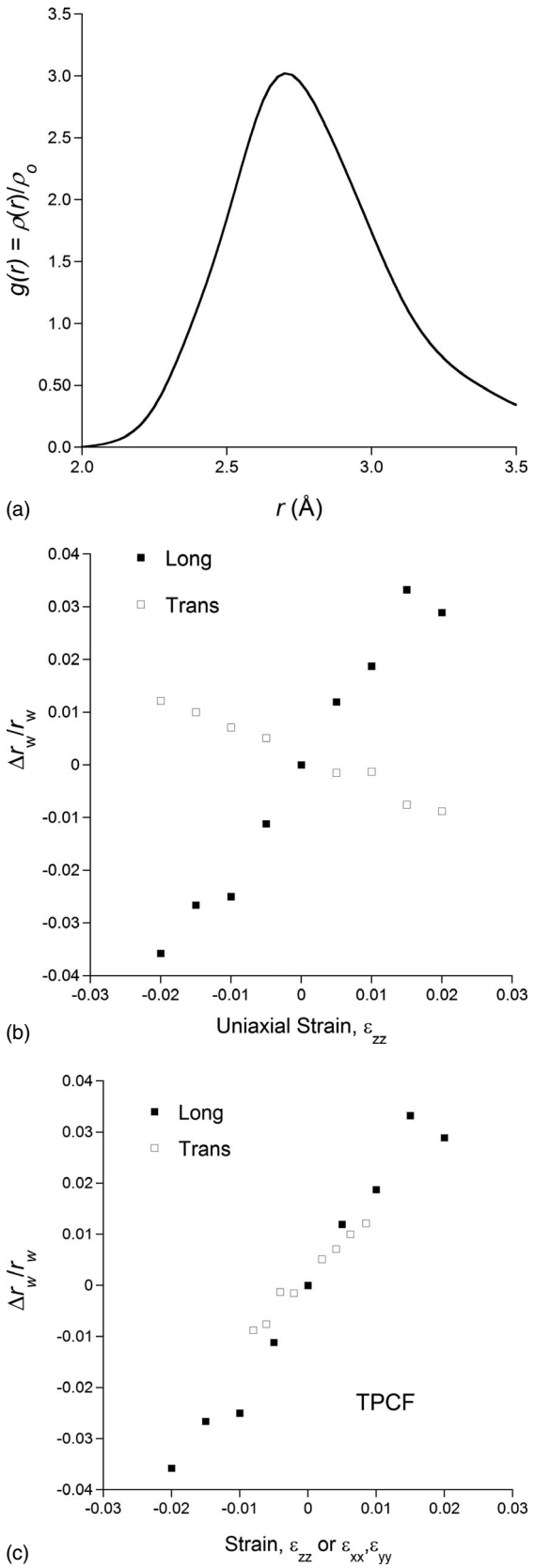

FIG. 4. (a) First peak in total $g(r)$ (for unstrained model) from MD simulations of $Cu_{64.5}Zr_{35.5}$ alloy. Normalized widths of first peaks in the directional total $g(r)$'s as a function of (b) applied uniaxial strain and (c) strain along the principal directions.

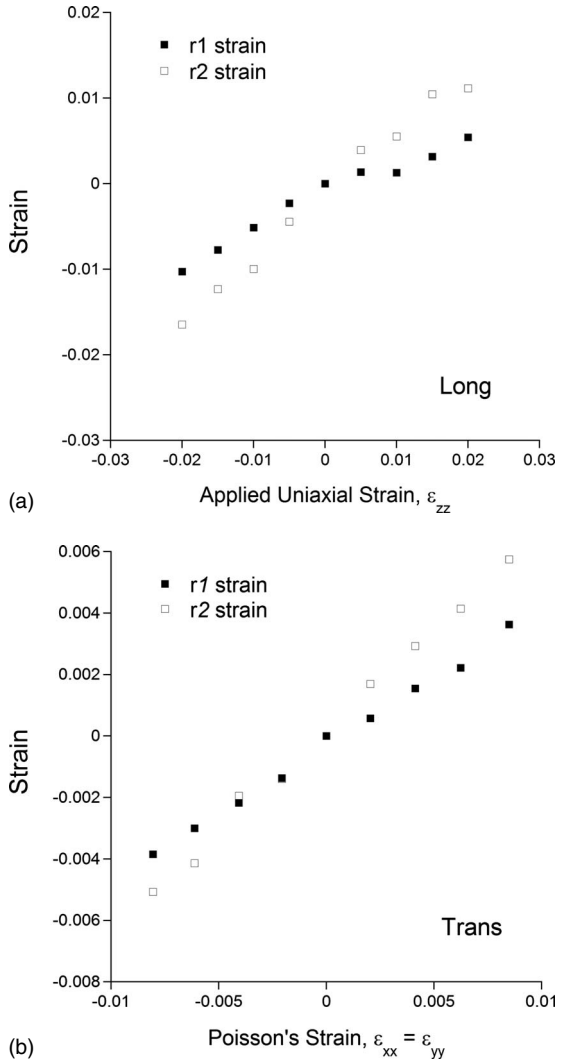

FIG. 5. Strain from r_1 and r_2 intercept points in the (a) longitudinal and (b) transverse directions as functions of applied and Poisson's strain, respectively, from MD simulation of the $Cu_{64.5}Zr_{35.5}$ model deformed uniaxially.

Therefore, the results from the MD simulations appear to correlate well with the experimental results, which indicate that during straining the peak width changes in the real-space distribution functions are dependent on the different elastic responses of the atomic correlations.

To overcome the limitations associated with measuring the width of the first peak in the total $g(r)$, we examined the widths of the first peaks in the partial-pair distribution functions, $g_{\alpha\beta}(r)$, for the $Cu_{64.5}Zr_{35.5}$ model deformed uniaxially. The peak widths of the $g_{\alpha\beta}(r)$'s, as functions of the strain along the principal directions for the $Cu_{64.5}Zr_{35.5}$ model deformed uniaxially are shown in Fig. 6. For the Cu-Cu and Cu-Zr partial-pair distribution functions, the widths of the first peaks decrease for tensile straining and increase for compressive straining. For the Zr-Zr partial-pair distribution function, the peak widths in the transverse direction appear to increase for compressive straining and decrease for tensile straining, while the peak widths in the longitudinal direction do not show and clear strain dependence. The large amount

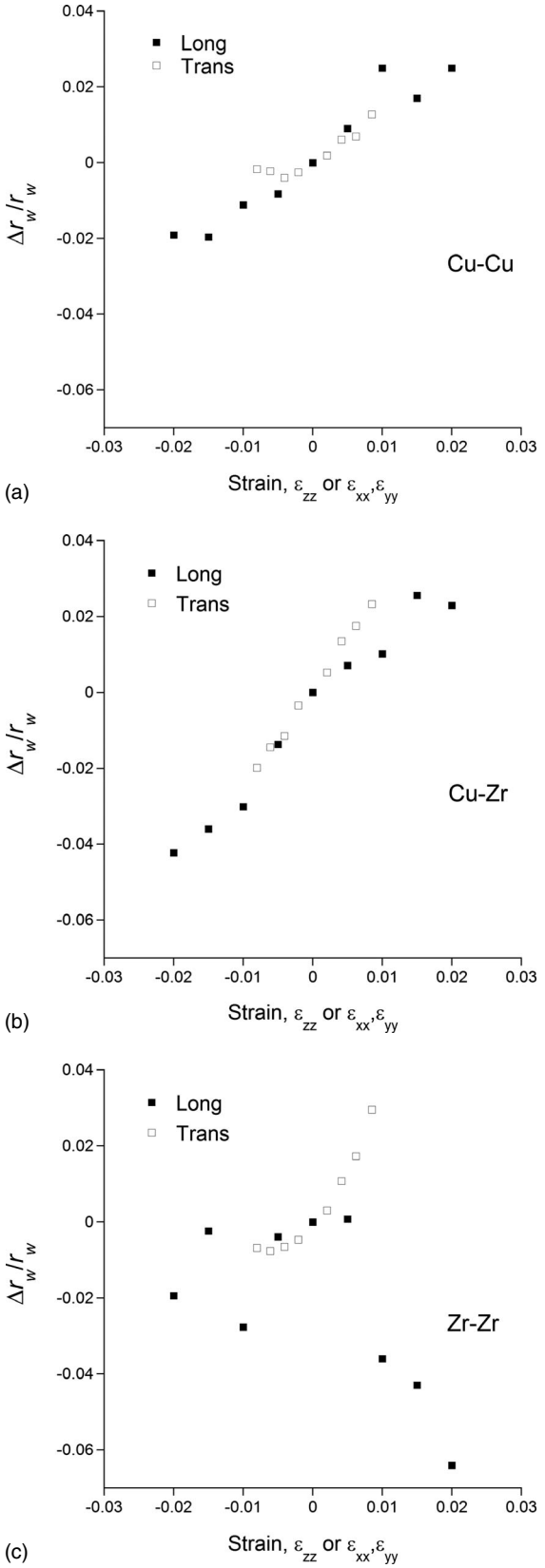

FIG. 6. Normalized widths of first peaks in (a) Cu-Cu, (b) Cu-Zr, and (c) Zr-Zr partial-pair distribution functions in the longitudinal and transverse direction as functions of strain along the principal directions from MD simulations of $Cu_{64.5}Zr_{35.5}$ alloy deformed uniaxially.

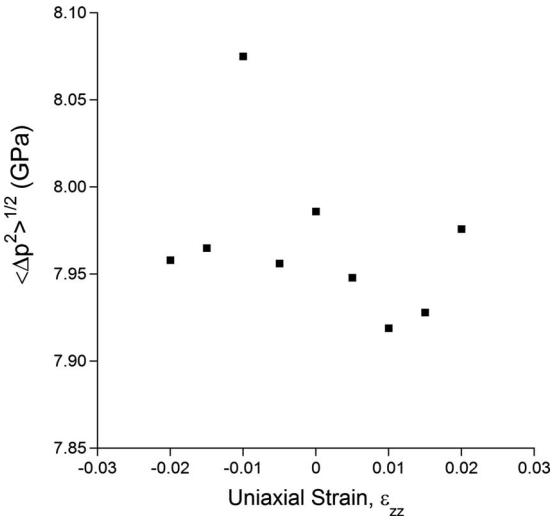

FIG. 7. Variance in local hydrostatic pressure, $\langle \Delta p^2 \rangle^{1/2}$, as a function of applied strain from MD simulations of uniaxial deformation of $Cu_{64.5}Zr_{35.5}$ alloy.

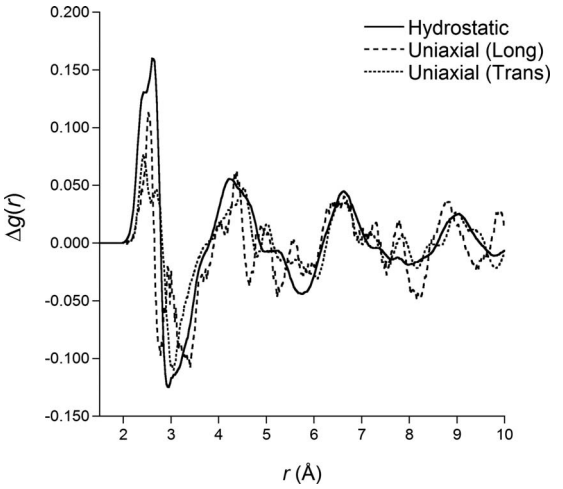

FIG. 8. Difference in total-pair distribution functions $[\Delta g(r) = g_\varepsilon(r) - g_o(r)]$ for unstrained ($\varepsilon = 0$) and strained ($\varepsilon = 0.01$) models of $Cu_{64.5}Zr_{35.5}$ deformed uniaxially and hydrostatically. For the uniaxial model, the strain refers to the uniaxial and Poisson's strain for the longitudinal and transverse directions, respectively.

of scatter in the measured peak widths in the longitudinal direction for $g_{Zr\text{-}Zr}(r)$ is likely due to the limited number of atomic pairs used to calculate the distribution function. As discussed above, only the atomic correlations that were oriented within $\pm 9°$ of the principal axes were used for calculating the directional distribution functions. Therefore, the number of atomic correlations analyzed is only a small fraction of the total amount of correlations. Since there is not a large fraction of Zr-Zr correlations in the $Cu_{64.5}Zr_{35.5}$ glass, the statistics for $g_{Zr\text{-}Zr}(r)$ are the worst of the different partial-pair distribution functions. The statistics should be significantly improved for the transverse direction (normal to applied strain), however, since the partial-pair distribution functions are calculated along two principal axes ($\varepsilon_{xx} = \varepsilon_{yy} = -\upsilon\varepsilon_{zz}$). In addition to the peak widths for the $g(r)$ functions, we also calculated the variance in the hydrostatic pressure, $\langle p^2 \rangle^{1/2}$ for the $Cu_{64.5}Zr_{35.5}$ glass deformed uniaxially. Figure 7, which shows $\langle p^2 \rangle^{1/2}$ as a function of applied uniaxial strain, reveals that $\langle p^2 \rangle^{1/2}$ shows no obvious strain dependence, suggesting that the peak width changes seen in the total and partial-pair distribution functions are not simply dependent on $\langle p^2 \rangle^{1/2}$.

C. Molecular dynamics simulations of hydrostatic deformation

The results from the MD simulations of uniaxial deformation reveal that the widths of the first peaks in the total- and partial-pair distribution functions exhibit strain dependence but the variance in the local hydrostatic pressure shows little, if any, dependence on the strain. In order to simplify the analysis and eliminate the statistics problems associated with calculating directional pair-distribution functions, we strained the same $Cu_{64.5}Zr_{35.5}$ model and the $Cu_{33.3}Zr_{66.7}$ model hydrostatically. For hydrostatic deformation, the pair-distribution functions should be the same in all three principal directions, and thus, the change in peak widths should be isotropic. The ability to use all of the atomic correlations for calculating the distribution functions significantly improves the statistics compared to the model deformed uniaxially. Moreover, utilizing hydrostatic straining ensures that the variance in the hydrostatic pressure will change during deformation. For a comparison between the models deformed uniaxially and hydrostatically, we calculated the difference in the partial-pair distribution functions, $\Delta g(r)$, for an unstrained model $[g_o(r)]$ and a strained model $[g_\varepsilon(r)]$, where Δg is defined as

$$\Delta g(r) = g_\varepsilon(r) - g_o(r). \tag{11}$$

Figure 8 shows the $\Delta g(r)$ function for the $Cu_{64.5}Zr_{35.5}$ glass deformed both uniaxially and hydrostatically. For the uniaxal models, the applied strain, ε_{zz}, was -0.01 for the strained model used to calculate $\Delta g(r)$ for the longitudinal direction and 0.0244 (ε_{xx}, $\varepsilon_{yy} = -0.01$) for the strained model used to calculate $\Delta g(r)$ for the transverse direction. The applied strain of 0.0244, which corresponds to a Poisson's strain of -0.01, is just below the yield strain determined from MD simulations of uniaxial deformation of the $Cu_{64.5}Zr_{35.5}$ glass. The $\Delta g(r)$ for the model deformed hydrostatically ($\varepsilon_{xx} = \varepsilon_{yy} = \varepsilon_{yy} = -0.01$) is significantly smoother than the models deformed uniaxially due to the fact that all the atomic correlations are included in the total $g(r)$ calculations. While the $\Delta g(r)$ function in the transverse direction for uniaxial loading is qualitatively similar to the $\Delta g(r)$ for the hydrostatically deformed model, the $\Delta g(r)$ in the longitudinal direction is noisier due to the decreased statistics. The results highlight the advantage of using hydrostatic deformation to examine the peak width changes during straining.

Figure 9(a) shows the widths of the first peaks of the total $g(r)$'s (determined by intercept method) as functions of applied hydrostatic strain for both the $Cu_{33.3}Zr_{66.7}$ and $Cu_{64.5}Zr_{35.5}$ glasses. Similar to the x-ray measurements and the MD simulations of uniaxial deformation of the $Cu_{64.5}Zr_{35.5}$ metallic glass, the peak widths for both amorphous Cu-Zr alloys decrease for compressive straining and

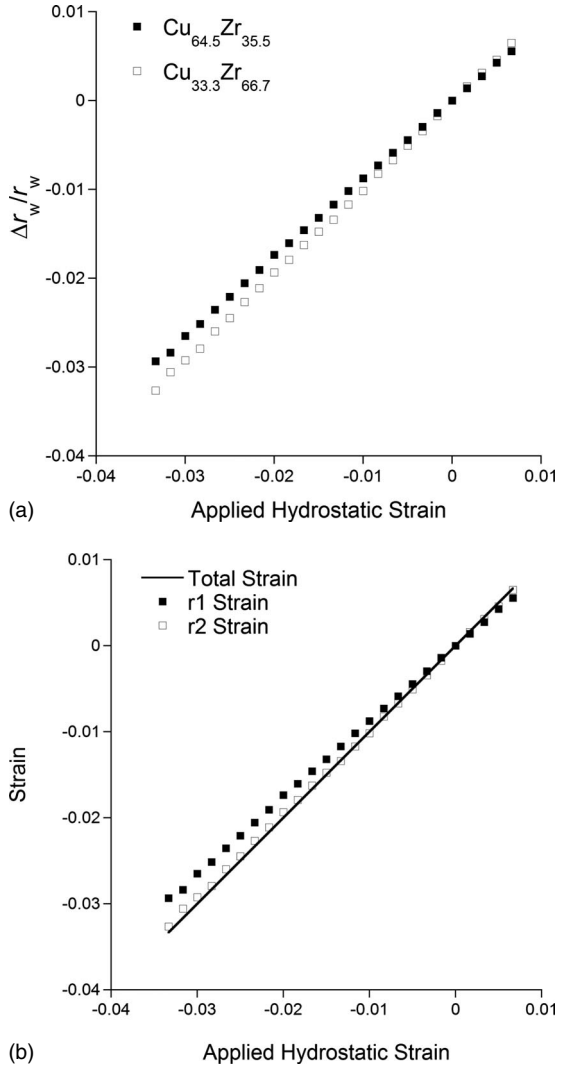

FIG. 9. (a) Normalized widths of first peaks of total $g(r)$'s as functions of applied hydrostatic strain from MD simulations of amorphous $Cu_{64.5}Zr_{35.5}$ and $Cu_{33.3}Zr_{66.7}$ alloys. (b) Strain from r_1 and r_2 intercept points along with total strain as functions of applied hydrostatic strain from MD simulations of $Cu_{64.5}Zr_{35.5}$ glass.

increase for tensile straining. Moreover, the MD simulations show that the peak width changes associated with hydrostatic deformation are primarily due to the different strain responses of the atoms corresponding to the r_1 and r_2 intercepts, Fig. 9(b). The change in the relative atomic separations for r_2 is larger than that for r_1, which would cause peak narrowing for compressive straining and broadening for tensile straining, consistent with Fig. 9(a). Therefore, we need to examine the peak widths of the individual partial-pair distribution functions to more accurately measure any dependence on $\langle \Delta p^2 \rangle^{1/2}$. Figure 10 shows the measured widths of the first peak in the $g_{\alpha\beta}(r)$ functions (measured by intercept method) as functions of applied hydrostatic strain for the two Cu-Zr glasses examined by MD simulations. For the $g_{CuCu}(r)$ and $g_{ZrZr}(r)$ functions, the widths of the first peaks increase for compressive straining and decrease for tensile straining. The peak widths of the $g_{CuZr}(r)$ functions exhibit much less obvious strain dependence. For the $Cu_{64.5}Zr_{35.5}$ alloy, the

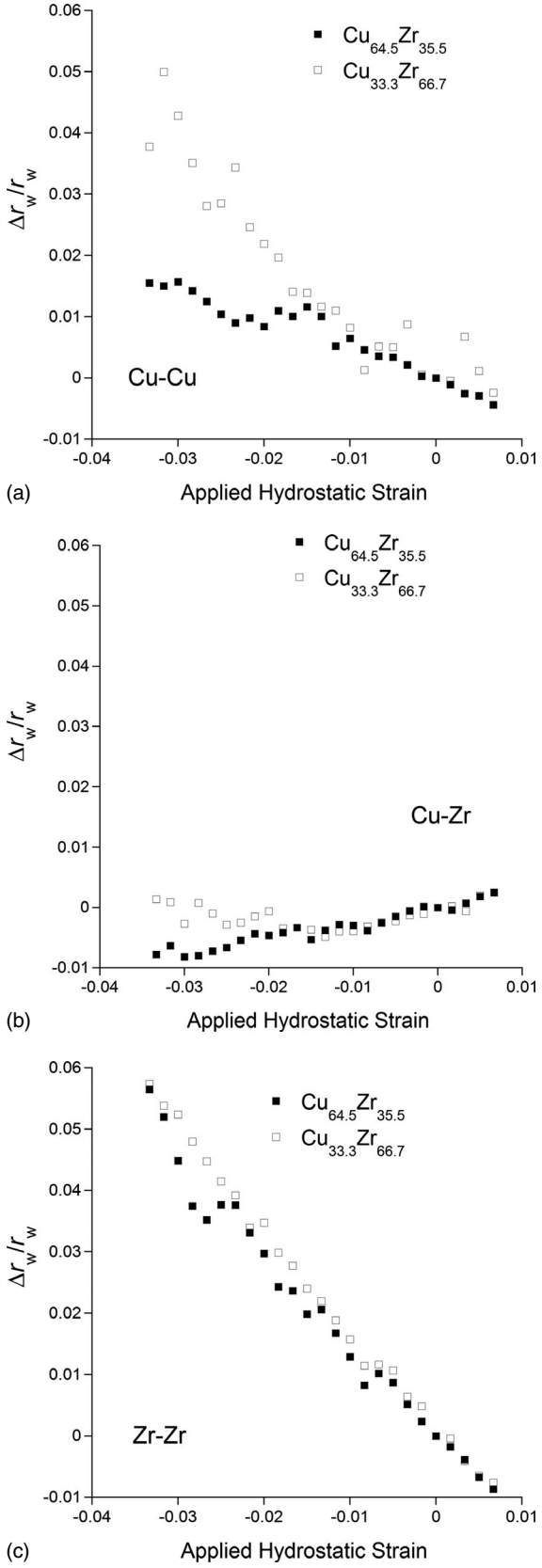

FIG. 10. Normalized widths of first peaks in (a) Cu-Cu, (b) Cu-Zr, and (c) Zr-Zr partial-pair distribution functions as functions of applied hydrostatic strain for Cu-Zr alloys examined using MD simulations.

peak width appears to decrease for compressive straining and increase for tensile straining, however, the $g_{CuZr}(r)$ peak widths for the $Cu_{33.3}Zr_{66.7}$ alloy do not show any definitive trend for compressive straining. It is interesting to note that the strain dependencies of the peak widths for the $g_{CuCu}(r)$ and $g_{ZrZr}(r)$ functions are opposite of that shown by the total $g(r)$ functions for the two Cu-Zr compositions. This further illustrates that the peak width changes seen in the total $g(r)$ functions are strongly dependent on the relative shifts in the positions of the partial-pair distribution functions during straining and not necessarily representative of the peak widths of the partial-pair functions.

From the MD simulations we find that the strain dependencies of the peak widths for the $g_{Cu\text{-}Cu}(r)$ from the $Cu_{64.5}Zr_{35.5}$ model deformed uniaxially and hydrostatically are the opposite of each other. The poorer statistics for the MD simulations of uniaxial deformation compared to the MD simulations of hydrostatic deformation might account for their different strain dependencies. Their opposite behavior might also be due to the important differences between the two deformation schemes. For instance, assuming linear elasticity, the change in the model volume for a given hydrostatic strain is larger than the change in volume for a uniaxial strain of the same magnitude. Since we are examining the partial-pair functions, we need to consider the changes in the average bond lengths of the different partial pairs in the first nearest-neighbor shells during straining. The peak widths were normalized to the change in bond lengths rather than the change in volume since the pair-distribution functions for uniaxial loading are not isotropic. A comparison of the widths of the first peaks in $g_{\alpha\beta}(r)$ for Cu-Cu and Cu-Zr (Zr-Zr is not included due to the limited statistics for uniaxial deformation) normalized to their average bond lengths is shown in Fig. 11. The results show that the strain dependencies of the $g_{\alpha\beta}(r)$ peak widths are not affected by normalization to the average bond lengths at each strain level, therefore, the deformation mode (uniaxial or hydrostatic) might be another factor that influences the $g_{\alpha\beta}(r)$ peak width changes during straining.

The preceding results demonstrate that with the exception of the Cu-Zr correlations for the $Cu_{33.3}Zr_{66.7}$ alloy, the peak widths of the partial-pair distribution functions exhibit clear strain dependencies for the hydrostatically deformed models. To further examine the nature of these peak width changes, we measured the changes in the relative atomic separations corresponding to the r_1 and r_2 intercepts. Using Eq. (4), we calculated the strain from the low-r (r_1) and high-r (r_2) intercepts where $g_{\alpha\beta}(r)=1$ for the first coordination shell as a function of applied hydrostatic strain for the $Cu_{64.5}Zr_{35.5}$ alloy, Fig. 12. We find that for all three partial-pair distribution functions, the strain calculated from r_1 is greater than the strain calculated from r_2 for both compression and tension. Similar behavior was observed for the $Cu_{33.3}Zr_{66.7}$ alloy (not shown). This difference in strains measured from the intercept points shows that for both compressive and tensile straining, the atoms that are initially slightly closer to the central atom (r_1 intercepts) in the first nearest-neighbor shell exhibit larger changes in their relative atomic separations during straining than the atoms slightly further away from the central atom (r_2 intercepts) in the first shell. This length-scale dependence of the strains should result in the $g_{\alpha\beta}(r)$ peak widths increasing for compressive straining and decreasing for tensile straining, which is indeed what we find for the Cu-Cu and Zr-Zr correlations. The peak width changes for the $g_{CuZr}(r)$ functions for the two alloys cannot be attributed to the different strain responses of r_1 and r_2, however. The results show that at least for the Cu-Zr correlations, the peak widths are not solely dependent on the length-scale-dependent atomic rearrangements.

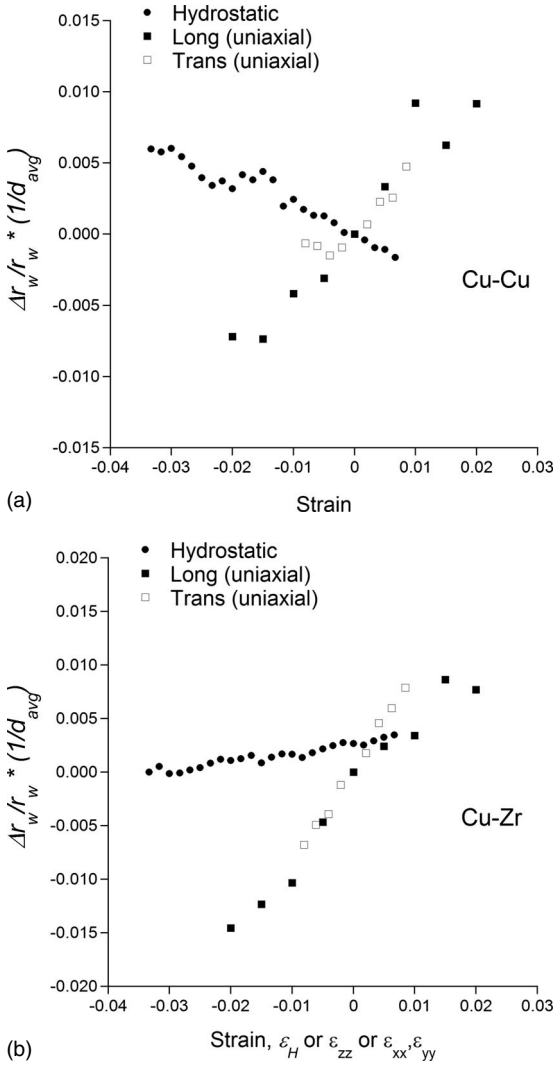

FIG. 11. Change in peak widths normalized to average bond length for Cu-Zr models deformed under applied uniaxial and hydrostatic strain. The normalized peak widths in (a) $g_{Cu\text{-}Cu}(r)$ and (b) $g_{Cu\text{-}Zr}(r)$ as functions of strain are shown.

To determine if the strain dependencies of the peak widths shown in Fig. 10 are dependent on the variance in the atomic-level hydrostatic pressure, we calculated $\langle \Delta p^2 \rangle^{1/2}$ for the two Cu-Zr glasses as a function of applied hydrostatic strain, Fig. 13. For the $Cu_{33.3}Zr_{66.7}$ alloy, $\langle \Delta p^2 \rangle^{1/2}$ increases with compressive straining and decreases with tensile straining while $\langle \Delta p^2 \rangle^{1/2}$ for the $Cu_{64.5}Zr_{35.5}$ alloy exhibits a small decrease for compressive straining and small increase for tensile straining. Therefore, from Figs. 10 and 13 we find that for the $Cu_{64.5}Zr_{35.5}$ alloy, the widths of the first peaks in

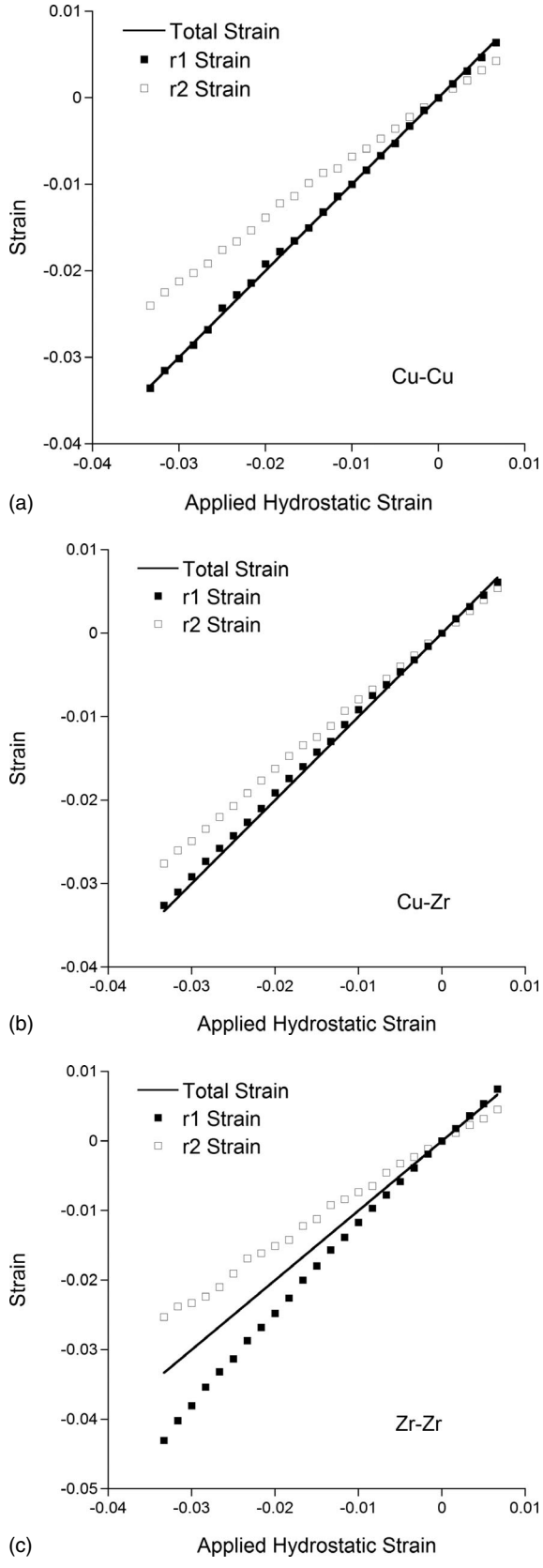

FIG. 12. Strains calculated from r_1 and r_2 intercept points of (a) Cu-Cu, (b) Cu-Zr, and (c) Zr-Zr partial-pair distribution functions for $Cu_{65.5}Zr_{35.5}$ alloy determined by MD simulations.

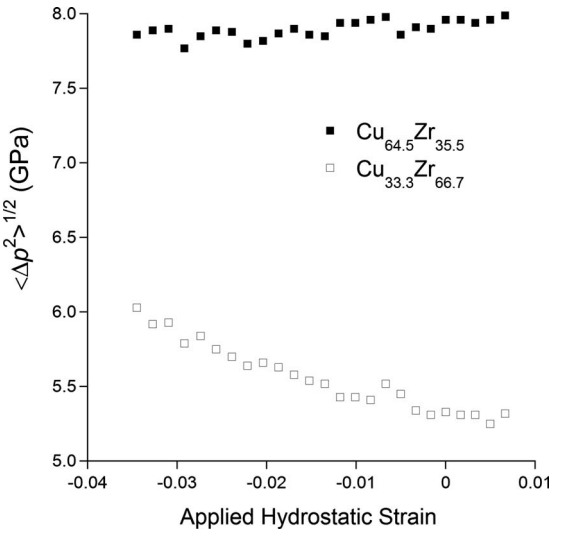

FIG. 13. Variance in local hydrostatic pressure, $\langle \Delta p^2 \rangle^{1/2}$, as a function of applied hydrostatic strain determined from MD simulations of Cu-Zr alloys.

the $g_{CuCu}(r)$ and $g_{ZrZr}(r)$ functions show opposite strain dependence than that of $\langle \Delta p^2 \rangle^{1/2}$. The strain dependence of the widths of the first peaks in the $g_{CuCu}(r)$ and $g_{ZrZr}(r)$ functions are the same as that of $\langle \Delta p^2 \rangle^{1/2}$ for the $Cu_{33.3}Zr_{66.7}$ alloy but the peak widths of the $g_{CuZr}(r)$ function do not appear to exhibit the same strain dependence as $\langle \Delta p^2 \rangle^{1/2}$. A summary of the strain dependencies of the variance in hydrostatic pressure and the distribution-function peak widths for the Cu-Zr alloys is presented in Table I. Given the different strain dependencies of the peak widths of the partial-pair distribution functions, it appears very unlikely that the peak widths are solely dependent on the variance in hydrostatic pressure, but rather the length-scale dependence of the atomic strains appears to play a significant role.

The MD simulations of amorphous Cu-Zr alloys subject to uniaxial and hydrostatic deformation reveal that the relationship between the width of the first peak in the $g_{\alpha\beta}(r)$ functions and the variance in the local hydrostatic pressure is complicated. Clearly the partial-pair correlations are affected differently by the applied strain. To exclude chemistry effects, we performed similar MD simulations on amorphous Al subject to hydrostatic strain. Obviously, the fact that amorphous Al can be obtained in the simulations highlights the limitations of the Ercolessi-Adams interatomic potential, but while the potential does not accurately capture the thermodynamic properties of real Al, it does provide a reasonable description of the structure of a single-component amorphous metal.[23] Since the first peak in the $g(r)$ for the Al glass is too asymmetric to be accurately fit with a single profile (Fig. 14), we used the intercept method to determine the peak width. The measured widths of the first peaks in $g(r)$ and $S(Q)$ as functions of applied hydrostatic strain are shown in Fig. 15(a). For the reciprocal-space data, $S(Q)$, the width of the first peak does not show any obvious strain dependence. It should be noted that Srolovitz and co-workers only examined the relationship between $\langle \Delta p^2 \rangle^{1/2}$ and the width of the first peak in the real-space distribution functions; therefore, it is unclear if similar behavior should be expected in

TABLE I. Summary of measured peak widths and variance in hydrostatic pressure as functions of applied stress (strain) for the two Cu-Zr alloys. C=compressive straining and T=tensile straining.

		$Cu_{64.5}Zr_{35.5}$	$Cu_{64.5}Zr_{35.5}$ (MD)		$Cu_{33.3}Zr_{66.7}$ (MD)
	Function	(X ray)	Uniaxial	Hydrostatic	Hydrostatic
Peak widths	$\langle \Delta p^2 \rangle^{1/2}$			↓C↑T	↑C↓T
	Total $G(r)$, $g(r)$	↓C↑T	↓C↑T	↓C↑T	↓C↑T
	$g_{Cu\text{-}Cu}(r)$		↓C↑T	↑C↓T	↑C↓T
	$g_{Cu\text{-}Zr}(r)$		↓C↑T	↓C↑T	?C↑T
	$g_{Zr\text{-}Zr}(r)$			↑C↓T	↑C↓T

the reciprocal-space data where the first peak does not primarily correspond to correlations in the first nearest-neighbor shell. For the real-space data however, the width of the first peak decreases for compressive straining and increases for tensile straining. This behavior is opposite of the strain dependence of $\langle \Delta p^2 \rangle^{1/2}$ [Fig. 15(b)], which increases with compressive straining and decreases with tensile straining. Similar to the partial-pair distribution functions for the Cu-Zr alloys, we find that the width of the first peak in $g(r)$ for the Al glass is also affected by length-scale-dependent atomic displacements. Figure 15(c), which shows the strain calculated from the two different intercept points for the first peak in $g(r)$, illustrates that the strain is not uniform among all the atoms. The larger strain determined from the r_2 intercept compared to the r_1 intercept would result in the strain dependence of the $g(r)$ peak widths that is seen in Fig. 15(a). Therefore, it appears that the length-scale dependence of the strain influences the peak widths of the distribution functions more than the variance in the local hydrostatic pressure for the Al glass we examined.

D. Peak width changes during high-temperature deformation

The x-ray and MD results show that the peak widths of the reciprocal- and real-space distribution functions are not solely dependent on the variance in the local hydrostatic pressure during elastic straining. Beyond the elastic limit, however, the peak widths should not be significantly affected by the different elastic responses of the partial-pair correlations since any additional strain is primarily plastic. Therefore, the peaks widths should be dependent on the structural order of the glass during plastic deformation. To examine this, samples of $Cu_{64.5}Zr_{35.5}$ metallic glass were homogeneously deformed in uniaxial compression at 425 °C at a constant strain rate of 10^{-4} s^{-1}. The measured width of the first peak in $S(Q)$ as a function of macroscopic displacement is shown in Fig. 16. The cross-head displacement is plotted since the macroscopic strain could not be accurately measured inside the furnace; the displacement, however, is directly proportional to the compressive strain. In the elastic regime the peak width in the longitudinal direction increases, which is consistent with what we observed for the room-temperature measurements, Fig. 2(b). Near the region where macroscopic yielding can be seen in the stress-displacement curve, the peak width exhibits a marked increase with increasing displacement. The increasing peak widths corresponding to yielding and subsequent flow softening can be more clearly seen in the zoomed in region shown in Fig. 16(b). The increase in the peak width is likely characteristic of structural disordering associated with the creation of flow defects. The flow softening following yielding is believed to be associated with an increase in flow defects and excess free volume.[27,28] As the creation and annihilation of free volume approach a dynamic equilibrium, the amount of excess free volume remains nearly constant and the stress-displacement (strain) response of the sample flattens out as shown in Fig. 16(a). In this region where the stress becomes essentially independent of strain, we see that the peak widths also show minimal dependence on the strain suggesting that the structural order is not significantly changing.

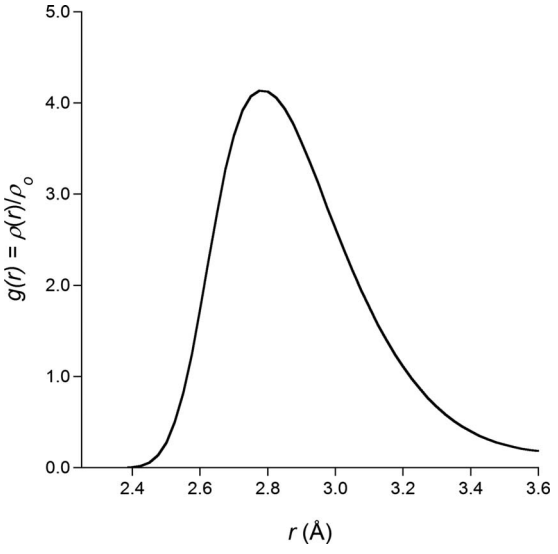

FIG. 14. First peak in $g(r)$ for amorphous Al determined using MD simulations

IV. CONCLUSIONS

In situ x-ray results show that determining the relationship between the peak widths of the reciprocal- and real-space distribution functions and the variance in the local hydrostatic pressure for metallic glasses subject to elastic straining is complicated. For an amorphous $Cu_{64.5}Zr_{35.5}$ alloy loaded in uniaxial compression and tension, the widths of the first peaks in the total $G(r)$ and $S(Q)$ are strongly dependent on the elastic responses of the different partial-pair correlations. The effects of the different bond stiffnesses are particularly

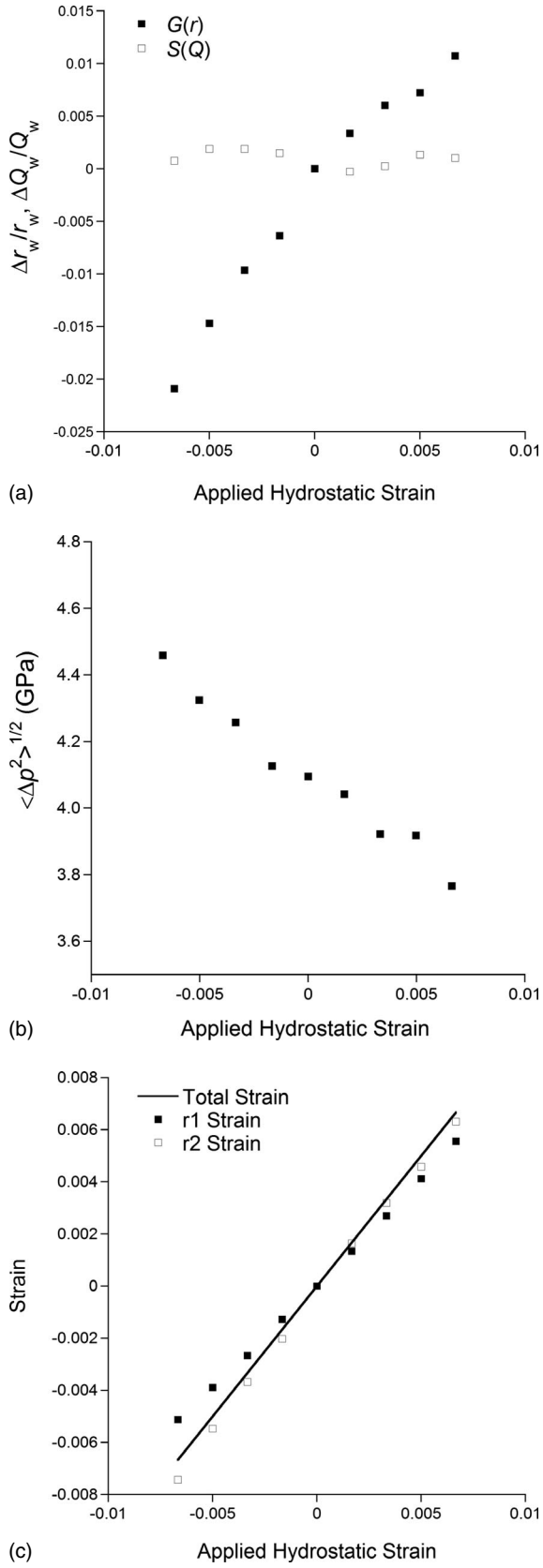

FIG. 15. (a) Normalized widths of first peaks in $g(r)$ and $S(Q)$, (b) variance in local hydrostatic pressure, and (c) atomic strains calculated from intercept points of first peak in $g(r)$ as functions of applied hydrostatic strain from MD simulations of Al glass.

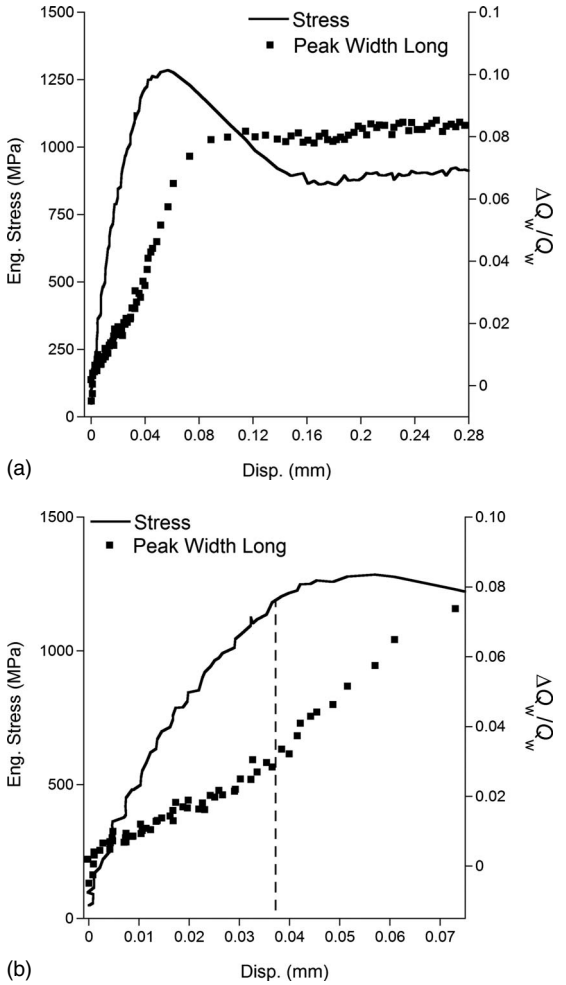

FIG. 16. (a) Macroscopic stress-displacement (strain) curves and normalized width of first peak in $S(Q)$ in longitudinal direction measured by x-ray scattering. (b) Zoomed in region showing transition from elastic to plastic flow. The dashed line indicates the onset of plastic flow in the macroscopic stress-displacement curve and the increase in peak width.

important when the peak width of the total $G(r)$ is measured using the intercept method. The results highlight the importance of examining the peak widths of the partial-pair functions.

Molecular dynamics simulations of amorphous Cu-Zr alloys deformed under applied uniaxial and hydrostatic strain show that the widths of the first peaks in the total- and partial-pair distribution functions do not necessarily exhibit the same strain dependencies as the variance in hydrostatic pressure. For the $Cu_{64.5}Zr_{35.5}$ model deformed uniaxially, we find that the strain dependence of the width of the first peak in the total $g(r)$ is consistent with experimental measurements. The variance in hydrostatic pressure, however, does not exhibit any obvious strain dependence. For the models that were hydrostatically strained, analysis of the strains calculated from the different intercept points of the first peak in the $g_{\alpha\beta}(r)$ functions reveal that the relative atomic separations of the atoms closest to the central atom change more than relative atomic separations of the atoms further away from the central atom in the first coordination shell. This

length-scale dependence of the atomic displacements can significantly affect the changes in the peak widths during elastic deformation. For the single component Al glass we find that the peak widths of $g(r)$ decrease for increasing variance in the hydrostatic pressure. Similar to the binary Cu-Zr alloys, the peak widths for the Al glass are also influenced by length-scale dependent changes in the relative atomic separations, however, the behavior is opposite of that exhibited by the Cu-Zr alloys.

Lastly, we find that for $Cu_{64.5}Zr_{35.5}$ metallic glass homogeneously deformed at 425 °C the peak width of the total $S(Q)$ exhibits a marked increase in the region corresponding to yielding and flow softening. The increase in peak widths with increasing plastic strain is likely characteristic of structural disordering associated with an increase in flow defects. As the concentration of flow defects approaches an equilibrium value, so does the measured peak width suggesting that during homogeneous plastic flow the peak widths are primarily dependent on the degree of structural order.

ACKNOWLEDGMENTS

The authors gratefully acknowledge D. Srolovitz (Yeshiva University) for the helpful discussions. This work was supported by the Office of Basic Energy Sciences, United States Department of Energy as follows: efforts at the Ames Laboratory were supported under Contract No. DE-AC02-07CH11358 and use of the Advanced Photon Source was supported under Contract No. DE-AC02-06CH11357.

[1] H. F. Poulsen, J. A. Wert, J. Neufeind, V. Honkimaki, and M. Daymond, Nature Mater. **4**, 33 (2005).
[2] T. C. Hufnagel, R. T. Ott, and J. Almer, Phys. Rev. B **73**, 064204 (2006).
[3] J. Das, M. Bostrom, N. Mattern, A. Kvick, A. R. Yavari, A. L. Greer, and J. Eckert, Phys. Rev. B **76**, 092203 (2007).
[4] T. Nasu, S. Takahashi, I. Ajiki, T. Usuki, Y. Onodera, M. Sakurai, Z. Wei, A. Inoue, B. He, W. J. Zhong, Z. Xie, and S. Q. Wei, J. Alloys Compd. **434-435**, 44 (2007).
[5] T. Wilson, B. Clausen, T. Proffen, J. Elle, and D. Brown, Metall. Mater. Trans. A **39**, 1942 (2008).
[6] T. Egami, K. Maeda, and V. Vitek, Philos. Mag. A **41**, 883 (1980).
[7] D. Srolovitz, K. Maeda, S. Takeuchi, T. Egami, and V. Vitek, J. Phys. F: Met. Phys. **11**, 2209 (1981).
[8] D. Srolovitz, T. Egami, and V. Vitek, Phys. Rev. B **24**, 6936 (1981).
[9] K. Maeda and S. Takeuchi, J. Phys. F: Met. Phys. **8**, L283 (1978).
[10] D. Srolovitz, K. Maeda, V. Vitek, and T. Egami, Philos. Mag. A **44**, 847 (1981).
[11] Materials Preparation Center, Ames Laboratory, U.S. DOE Basic Energy Sciences, Ames, IA, USA, available from, www.mpc.ameslab.gov
[12] A. P. Hammersley, S. O. Svensson, M. Hanfland, A. N. Fitch, and D. Hausermann, High Press. Res. **14**, 235 (1996).
[13] X. Qiu, J. W. Thompson, and S. J. L. Billinge, J. Appl. Crystallogr. **37**, 678 (2004).
[14] C. W. Dwiggins and D. A. Park, Acta Crystallogr., Sect. A: Cryst. Phys., Diffr., Theor. Gen. Crystallogr. **27**, 264 (1971).
[15] B. E. Warren, *X-Ray Diffraction* (Dover, New York, 1990).
[16] R. Serimaa, T. Pitkanen, S. Vahvaselka, and T. Paakkari, J. Appl. Crystallogr. **23**, 11 (1990).
[17] B. J. Thijsse, J. Appl. Crystallogr. **17**, 61 (1984).
[18] *International Tables of Crystallography*, edited by A. J. C. Wilson (Kluwer Academic, Dordrecht, 1995), Vol. C.
[19] W. Dmowski and T. Egami, J. Mater. Res. **22**, 412 (2007).
[20] M. I. Mendelev, D. J. Sordelet, and M. J. Kramer, J. Appl. Phys. **102**, 043501 (2007).
[21] M. I. Mendelev, D. K. Rehbein, R. T. Ott, M. J. Kramer, and D. J. Sordelet, J. Appl. Phys. **102**, 093518 (2007).
[22] F. Ercolessi and J. B. Adams, Europhys. Lett. **26**, 583 (1994).
[23] M. I. Mendelev, J. Schmalian, C. Z. Wang, J. R. Morris, and K. M. Ho, Phys. Rev. B **74**, 104206 (2006).
[24] W. L. Johnson and K. Samwer, Phys. Rev. Lett. **95**, 195501 (2005).
[25] G. Knuyt and L. M. Stals, Philos. Mag. B **64**, 299 (1991).
[26] E. Pineda, Phys. Rev. B **73**, 104109 (2006).
[27] P. De Hey, J. Sietsma, and A. van den Beukel, Acta Mater. **46**, 5873 (1998).
[28] M. Heggen, F. Spaepen, and M. Feuerbacher, J. Appl. Phys. **97**, 033506 (2005).